3D OPEN STRUCTURE CONTINUOUS-FIBRE COMPOSITE PARTS: YARN PATH OPTIMIZATION

Liao, C[1], and Robitaille, F[1]*
[1]Department of Mechanical Engineering, University of Ottawa, Canada
* francois.robitaille@uottawa.ca

Keywords: *Specific stiffness, Emerging manufacturing processes*

ABSTRACT

The advantages of polymer-matrix fibre-reinforced composites (PMFRC) over metal alloys in terms of specific stiffness and strength are well documented. However, ongoing developments in additive manufacturing processes for metals have enabled the production of parts that rival or better PMFRC parts in terms of specific properties, once the part is considered as opposed to its constituent material. Furthermore, whilst powder-based additive manufacturing processes are used for targeted applications with less cost constraints, wire-based processes enable more affordable production of metal parts and challenge market penetration for some PMFRC parts made produced traditional processes. Efforts were made in producing continuous fibre PMFRC open structures such as isogrids and truss structures. In parallel, yarn deposition technologies were brought to market. Most available deposition technologies feature layered structures where yarns extend in parallel planes. Whilst such structures are highly reminiscent of traditional textile and prepreg laminates, they stand in contrast with the geometry of additively manufactured metal parts where material is deposited along 3D paths that maximise specific structural performance for a given set of loading cases. This paper discusses the optimisation of non-periodic open structure continuous-fibre PMFRC parts where yarns extend along 3D paths that maximize specific structural performance of the resulting part for specific load cases. The paper focuses on optimisation of the geometry of the dry yarn structure using a steepest ascent (SA) method and calculation of structural performance as a PMFRC part using finite elements (FEA).

1 INTRODUCTION AND LITERATURE

PMFRC are structural materials of choice for numerous demanding applications because of their exceptional specific mechanical properties and relative ease of manufacturing, especially in small series. These major advantages have lead to prevalence in aerospace where more than 50% of the structure of aircraft are routinely made of PMFRCs.

The last decades have seen the parallel emergence of additive manufacturing processes and parts made of polymers and, crucially here, metal alloys. Additive manufacturing enables the production of parts featuring geometry that cannot be made using subtractive processes such as CNC machining. The processes also enable economic production of trellis or lattice parts where topological optimization leads to material deposited only along paths of high stresses under specific load cases. These technologies result in parts that are highly efficient on a mass basis [1].

PMFRC manufacturing processes such as liquid moulding, filament winding, advanced tape placement and most others are inherently additive in nature. Despite this, true topology optimization has not happened with PMFRC, for two reasons [2]. First, the usage of continuous yarns in structural PMFRC restricts flexibility in yarn orientations. Printed PMFRC parts typically feature short fibres or layered continuous yarns [3] that can be oriented optimally in 2D, but less so in 3D along paths of higher normal stress [4]. Secondly, most industrial PMFRC processes do not

enable routine production of optimized trellis or lattices structures. Some examples were reported but the resulting truss-like structures are typically defined within simple geometric envelopes and feature a repeating structural unit [5], or develop from shells into isogrids [6]. Few examples of non-repeating structures were reported [7]. As a result, whilst PMFRC do outperform metal alloys in terms of specific properties, in the current state of technology additively manufactured structures made from alloys can outperform additively manufactured structures made from PMFRCs. PMFRC parts remain largely limited to continuous shell geometries from limitations in manufacturing processes.

The work reported in this paper aims at bringing topology optimization to PMFRC parts. Open structure continuous-fibre PMFRC parts are designed by optimizing the geometry of a non-periodic interlaced dry reinforcement defined in 3D through adjustments made to individual yarn or yarn group tensions. First, the positions of interlacing points in a dry yarn reinforcement structure where yarns are tensioned individually are calculated using a SA procedure. Then, the resulting 3D PMFRC part is subjected to loads and boundary conditions. PMFRC material extending between interlacing points is modelled as bars subjected to tensile/compressive loading, and displacements at points of application of external loads are calculated using FEA. These displacements are minimized through another SA procedure where yarn tensions are progressively adjusted, leading to an optimized continuous fibre PMFRC part.

The work reported in this paper constitutes the first step towards the development of the design and manufacturing process. The paper focuses on SA identification of the geometry of interlaced dry reinforcements and positions of interlacing points under set yarn tensions; SA procedure for minimizing displacements at loading points through finite element analysis (FEA) and adjustment of yarn tensions; equilibrium at interlacing points and identification of yarn paths; and a mention of further steps to be undertaken and completed toward PMFRC part production.

2 DRY REINFORCEMENT AND EQUILIBRIUM STEEPEST ASCENT

SA methods are used for identifying an optimum of a function. The methods presuppose that the direction of fastest increase or decrease of the response at a given point is the direction towards the optimum. Therefore, determining the gradient at that point sets the direction along which to probe further. Two main aspects of the method are the calculation of gradients and the size of steps towards the next probing point. As gradients remain large and positive, search continues along the current direction. Once the gradient becomes negative, search direction changes along with step size. Convergence is reached when the difference between successive iterations is sufficiently small.

The goal here is to design an open structure where yarns interlace within the part envelope in a way that reduces strains under a set load case for a given total material mass. The pre-set part envelope is defined along with an arbitrary number of yarns and their end positions, as well as pre-equilibrium and pre-optimization positions of dry yarns interlacing points. Eventually, dry yarns interlacing points are displaced to optimal positions by adjusting tension levels applied at yarn ends; frictionless interlacing is assumed. Two different instances of the SA method are implemented for doing so. The first instance, labelled equilibrium SA, is an inner loop used for identifying interlacing point equilibrium positions for the dry yarns under set tensions, irrespective of any loads applied eventually on the PMFRC structure. Figure 1 shows a simple 2D non-triangulated example where grey yarn 1 and red yarn 2 interlace, yarn 2 and yellow yarn 3 interlace, and yarn 3 and blue yarn 4 interlace. Numbers show dry yarn ends connecting to tensioning devices. Green circles identify other envelope points where dry yarns are redirected into the part. Part envelope and boundary conditions are defined by the case. Initial interlacing is currently defined arbitrarily. Lengths of dry yarns in the envelope are variable and depend only on applied yarn tensions and resulting interlacing point equilibrium positions; therefore, PMFRC part mass will vary upon optimization. Equilibrium SA is used for minimizing total strain energy in yarns as a function of the *x*, *y* and *z* coordinates of all interlacing points, leading to equilibrium positions. All three coordinates of all interlacing points are probed in turn until convergence is reached.

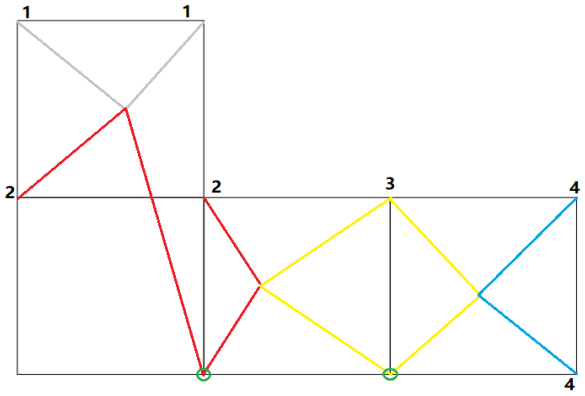

Figure 1. Basic 2D example showing envelope, boundary points, contact points, yarns and interlacing points

Open structures 3D PMFRC parts discussed below are more complex than shown in Figure 1: all structures are triangulated, more than two yarns may interlace at any interlacing point, equilibrium at interlacing points is verified systematically, and some segments extending between two interlacing points may feature more than one yarn.

3 PMFRC STRUCTURE, FEA AND STRUCTURAL STEEPEST ASCENT

FEA is used for determining displacements at points of external load application, along with internal stresses and strains in the PMFRC structure. Results are used in a second SA optimization cycle labelled structural SA. Structural SA includes both FEA analysis and equilibrium SA; specific stiffness of the PMFRC open structure part is increased for a specific load case, through looping the dry yarn tensions, re-equilibrating, and re-assessing using FEA.

In this early version of the work, PMFRC segments extending between two boundary, contact and/or interlacing points are modelled as bars subjected to tension/compression only; torsion and bending are not considered. All structures are triangulated and all bars form tetrahedra to limit deformations in the PMFRC part under load. The stiffness equation for all bar member elements is applied, Equation 1:

$$[K^a]\{U^a\} = \{F^a\} \tag{1}$$

where $\{F^a\}$ is the vector of applied loads including reactions at fixed boundary points and $[K^a]$ is the stiffness matrix for bar elements, Equation 2 where *E, A* and *L* are the elastic modulus, cross-section area and bar length, and $l = \frac{x_j - x_i}{L}$, $m = \frac{y_j - y_i}{L}$ and $n = \frac{z_j - z_i}{L}$. $\{U^a\}$ is the vector of nodal displacements to be calculated. Under applied forces and knowing the matrix representing the entire structure, solving leads to nodal displacements.

$$[K^a] = \frac{AE}{L}\begin{bmatrix} l^2 & lm & ln & -l^2 & -lm & -ln \\ lm & m^2 & mn & -lm & -m^2 & -mn \\ ln & mn & n^2 & -ln & -mn & -n^2 \\ -l^2 & -lm & -ln & l^2 & lm & ln \\ -lm & -m^2 & -mn & lm & m^2 & mn \\ -ln & -mn & -n^2 & ln & mn & n^2 \end{bmatrix} \tag{2}$$

Once nodal displacements are determined, all element properties can be acquired. For example, at element *e*, the nodal displacements are $\{U^e\}$, which is combined with rotation matrix $[T^e]$ to report the calculation to the element, hence axial elongation $\{\delta\}$ is obtained. The material is realistically assumed to be linear elastic, hence axial strain is

$\varepsilon = \frac{\delta}{L}$, and stress along the element is $\sigma = E * \varepsilon$. Subsequently, axial internal forces are determined as $F = A * \sigma$. After verifying all loads against elastic limits, buckling and failure criteria, structural stiffness of the part is obtained.

FEA analysis and equilibrium SA are combined within structural SA. Structural SA varies dry interlacing yarn tensions that are equilibrated by equilibrium SA, to create a new PMFRC open structure part analysed by FEA. Corresponding displacements are identified, and the open structure part is optimized in terms of specific stiffness for a given load case. Optimization does account for total mass, which is trivial as total yarn length is known.

4 EXAMPLE CASES

Introductory example 1 is defined in a 10 cm side length cube and features 3 continuous yarns and 1 interlacing point, Figure 2. The structure is delimited by 12 vertices #3, #8, #11-15, #17, #22-25 corresponding to the edges of the cube/part envelope. This is anecdotal to this case; no requirement is set on external vertices of the envelope. Yarns shown in magenta (yarn 1), blue (yarn 2) and black (yarn 3) extend uninterrupted as segments #1-5, #6-10 and #11-26. Yarn paths were selected arbitrarily with the only imperatives of producing a triangulated structure with stable interlacing points. Yarn entry and exit points are shown by coloured arrows. Yarns undergo different tensions at these points; the interlacing point position is altered accordingly. An optimized open structure PMFRC part with different internal geometry will be obtained within the same part envelope and external boundary points.

In its initial pre-equilibrium and pre-optimization configuration, the interlacing point is positioned arbitrarily at the centre of the domain, leading to 8 diagonal yarn segments #1, #2, #4-7, #9, #10 interlacing. The domain within the part envelope is divided into 6 pentahedra, each one then divided into 2 tetrahedra for triangulation, leading to 12 tetrahedra with identical dimensions in their initial configuration. The loading case was set arbitrarily by anchoring the ends of all 4 upper vertices marked by 4 red triangles, and applying a vertical downward 50 N force in the lower right corner (x = 10, y = 0). Bar stiffness and bar section were set at 0.2E9 N/m and 5E-6 m2.

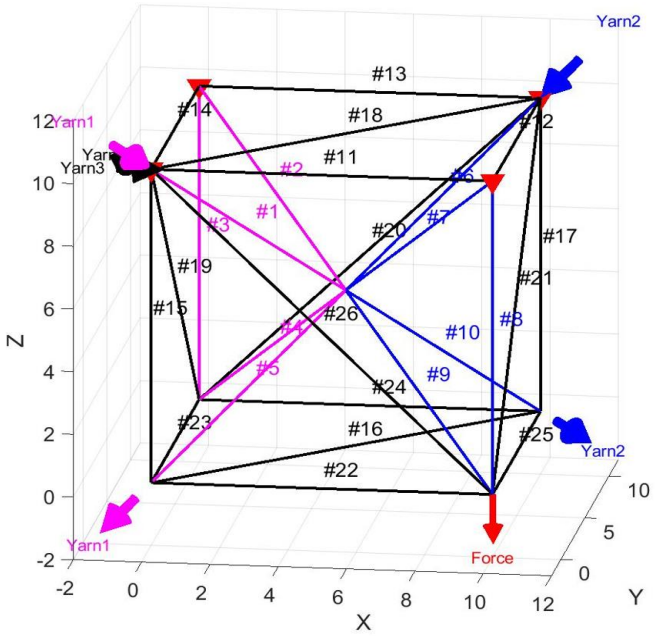

Figure 2. Interlacing diagram for pre-equilibrium 3D structure example 1 featuring 3 yarns and 1 interlacing point

Pre-optimization tensions were all set to 10N leading to central interlacing point (x = 5, y = 5, z = 5), Figure 3a). Dotted lines show the initial structure whilst coloured continuous lines show the deformed structure under load. Anecdotally, this is the same position as the arbitrary initial position – to be clear, the position stays the same post-equilibrium SA but pre-optimization of yarn tensions and structural SA. Applying the load leads to a pre-optimization vertical displacement of 0.3995 cm at the point of application, with largest tension in bar #8 nearing 40 N.

Structural SA leads to tensions in yarns 1 and 2 equal to 5 N and 15 N respectively, the ratio of 3 being set as an arbitrary limit. Results in Figure 3b) show vertical displacement at the point of load application of 0.3897 cm, with largest tension in bar #8 reduced slightly to below 39 N. Displacement was reduced by 2.45% for an increase in mass of 1.15% for minor improvements in structural and specific structural stiffness, Table 1. Improvements gained through optimization are very limited for example 1, for two reasons. First, bar #8 extends between the point of load application and one anchoring point along the line of action of the load, and bar #21 extends in a plane defined by the line of action of the load and two anchoring points. Consequently, contributions to stiffness from other bars are minimal for example 1. Secondly, the ratio of yarn tensions was artificially limited to replicate similar restrictions that will arise in manufacturing. This, in turns, limits possible displacements of the interlacing point for example 1.

Table 1. Pre-and post-optimization displacements and bar lengths, example 1

	Initial, pre-optimization	Optimized	Δ
Applied load	50 N, vertical down	50 N, vertical down	-
Displacement (cm)	0.3995	0.3897	-2.45%
Total bar length (cm)	274.3	277.3	+1.15%

Example 2 is defined as two similar cubes, Figure 4a) and features 4 continuous yarns with yarns 1, 2 and 3 as above and yarn 4 in red extending uninterrupted as yarn segments #1-10, #11-20, #21-34 and #35-47. All yarn paths were selected arbitrarily for a triangulated structure with stable interlacing points. Black yarn 3 and red yarn 4 overlap over segment #32, doubling stiffness. The part is delimited by 16 vertices #3, #8, #13, #18, #21-24, #30, #34-38, #44, #47 on its envelope edges. Initial, pre-equilibrium, pre-optimization configuration features two interlacing points positioned arbitrarily at the centres of the cubes leading to 16 diagonal yarn segments #1-2, #4-7, #9-12, #14-17, #19-20 interlacing. The part envelope was divided into 12 pentahedra, each divided into 2 tetrahedra for triangulation leading to 24 tetrahedra with identical dimensions in their initial configuration.

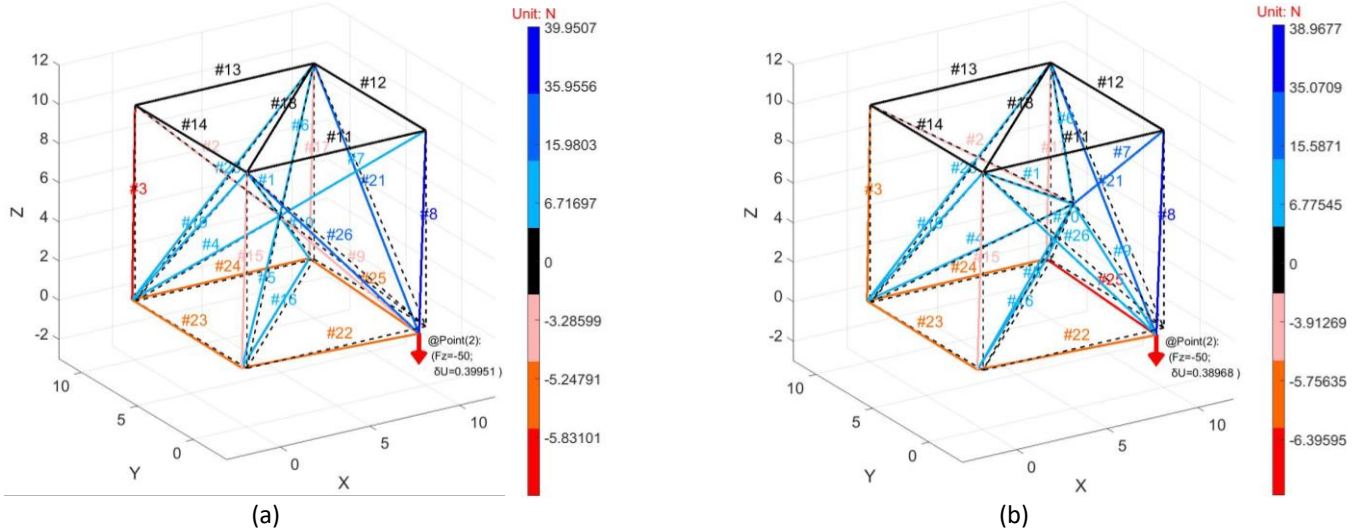

(a) (b)

Figure 3. Displacements and force distributions in non-optimized (a) and optimized (b) parts, example 1

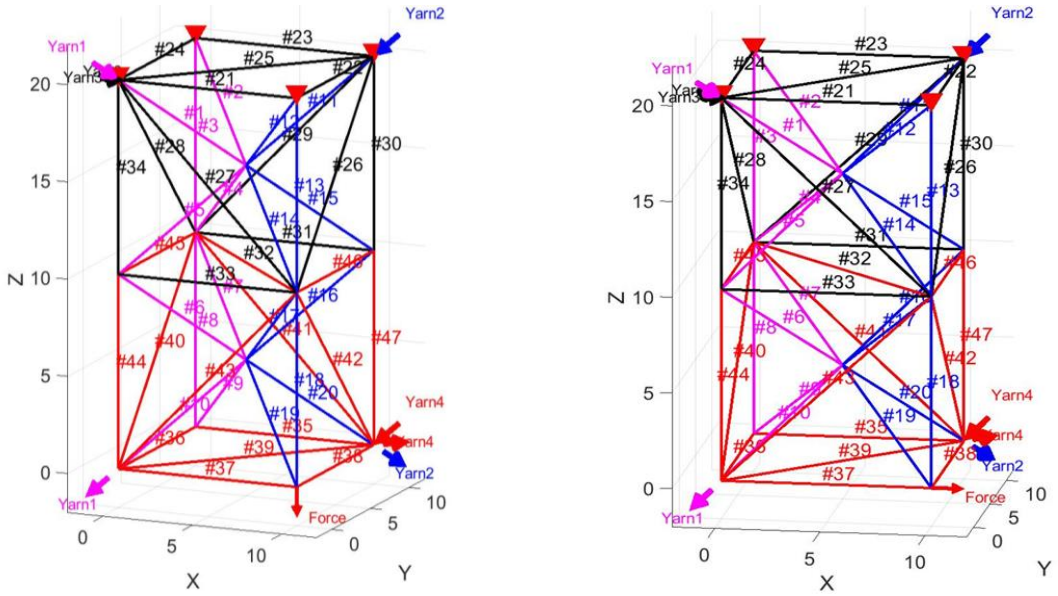

Figure 4. Interlacing diagram for pre-equilibrium 3D structure example 2 featuring 4 yarns and 2 interlacing points for (a) load case 1 and (b) load case 2

In load case 2.1, all 4 vertex ends in the upper plane marked by red triangles were anchored and a vertical downward 50 N load was applied in the lower right corner (x = 10, y = 0). Bar stiffness and section remained the same. Initial tensions set to 10 N pre-structural SA lead to central interlacing points in each cube (x=5, y=5, z=5), (x=5, y=5, z=15), Figure 5a). Pre-optimization vertical displacement was 0.7917 cm at load application point, with largest tension in bar #18 slightly above 45 N. Structural SA leads to tensions in yarns 1 and 2 of 5 N and 15 N respectively, artificially limited to 1:3 as above, Figure 5b). Displacement reduced to 0.7511 cm and largest tension in bar #18 reduced to 42.7 N. Displacement was reduced by 5.12% and length increased by 1.22%, Table 2. The change in length and mass is not the same as for example 1, because example 2 is not exactly twice the structure in example 1.

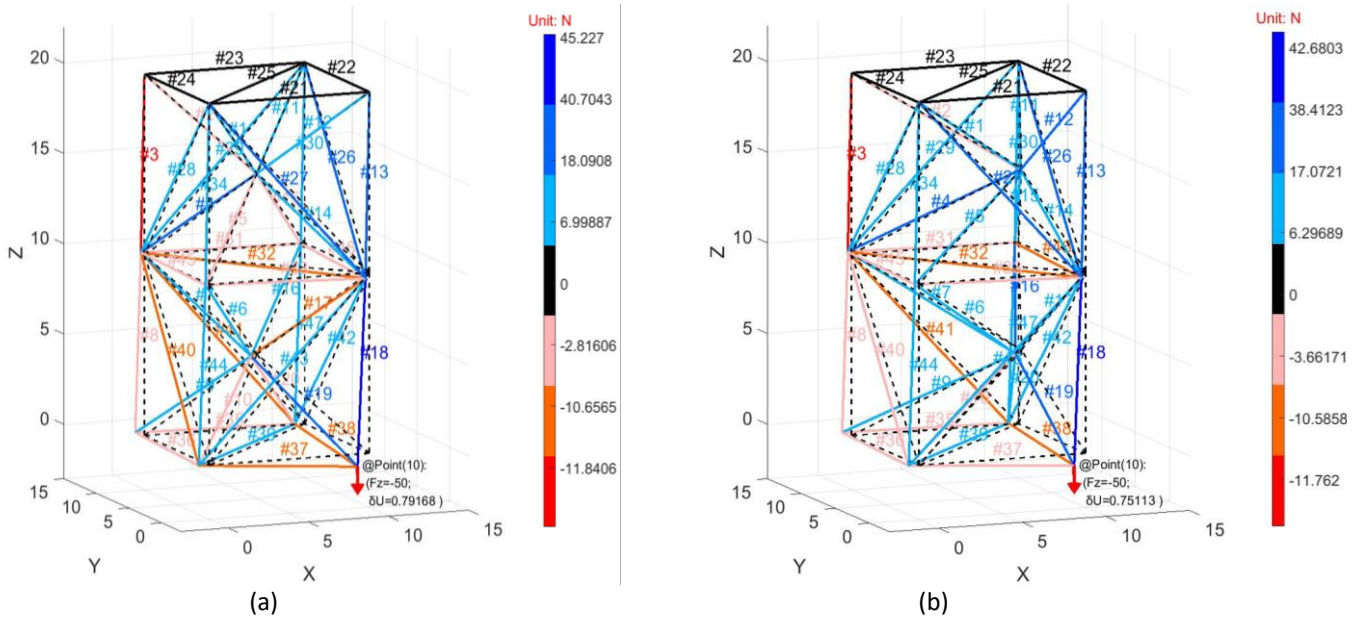

Figure 5. Displacements and force distributions in non-optimized (a) and optimized (b) parts, example 2, load 2.1

Table 2. Pre-and post-optimization displacements and bar lengths, example 2, load case 2.1

	Initial, pre-optimization	Optimized	Δ
Applied load 2.1	50 N, vertical down	50 N, vertical down	-
Displacement (cm), load 2.1	0.7917	0.7511	-5.12%
Total bar length (cm), load 2.1	508.3	514.5	+1.22%

Load case 2.2 was similar, with a force applied horizontally along positive axis *x*, Figure 6. Initial 10 N pre-optimized tensions lead to a horizontal displacement of 2.9838 cm at the point of application, Figure 6a), with largest tension in bar #3 nearing 39 N. Structural optimization reduced horizontal displacement to 2.8016 cm and largest tension in bar #3 to 35.3 N, Figure 6b). Displacement reduced by 6.10% for an increase in yarn mass of 1.22%, Table 3. Improvements in stiffness and specific stiffness were larger than for example 1. They are limited but not negligible, despite limitations imposed on tension ratios.

Table 3. Pre-and post-optimization displacements and bar lengths, example 2, load case 2.2

	Initial, pre-optimization	Optimized	Δ
Applied load 2.2	50 N, horizontal x+	50 N, horizontal x+	-
Displacement (cm), load 2.2	2.9838	2.8016	-6.10%
Total bar length (cm), load 2.2	508.3	514.5	+1.22%

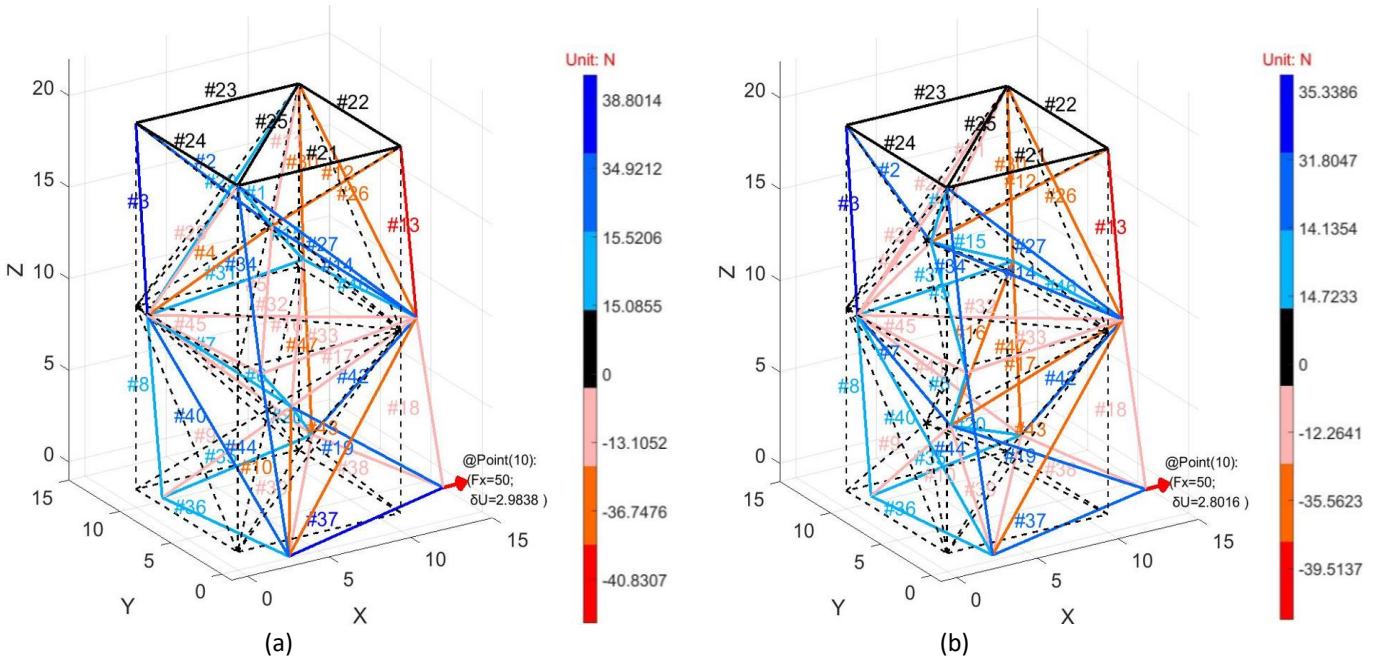

(a) (b)

Figure 6. Displacements and force distributions in non-optimized (a) and optimized (b) parts, example 2, load 2.2

Further optimization is possible by freeing contact point motion. Load cases 2.3 and 2.4 feature the same downward load as case 2.1, Figure 7. In case 2.3 mid-plane contact points A, B, C and D could move along *z*. Displacement and largest bar tension were reduced to 0.7166 cm and 46.2 N, bar #18. Movements of all boundary points along *z* reduced displacement 9.49% for a mass increase of 1.60%, Table 4. In case 2.4, points B & D were further allowed, arbitrarily, to move along *x* and *y* respectively. Displacement and largest bar tension were reduced to 0.5869 cm and 36.7 N, bar #18. Case 2.4 leads to a major reduction in displacement nearing 26% for a mass increase of 0.42%. However, part envelope was changed for load case 2.4, which might be acceptable in practical applications, or not.

Table 4. Pre-and post-optimization displacements and bar lengths, example 2, load cases 2.3 and 2.4

	Initial, pre-optimization	Optimized	Δ
Applied load 2.3	50 N, vertical down	50 N, vertical down	-
Displacement (cm), load 2.3	0.7917	0.7166	-9.49%
Total bar length (cm), load 2.3	508.3	516.4	1.60%
Applied load 2.4	50 N, vertical down	50 N, vertical down	-
Displacement (cm), load 2.4	0.7917	0.5869	-25.87%
Total bar length (cm), load 2.4	508.3	510.4	0.42%

Example 3 features 4 similar cubes and 2 triangular prisms, Figure 8. Yarns 1 to 7 form segments #1-10, #11-20, #21-30, #31-40 and #41-44 for yarns 1 to 5, used for positioning interlacing points under different tensions. Yarns 6 and 7 make segments #45-87 and #88-105. The structure is delimited by 21 vertices. Six 6 interlacing points positioned arbitrarily at the centres of the cubes and prisms lead to 44 diagonal yarn segments #1-44 interlacing. Part envelope is divided into 64 tetrahedra with identical initial dimensions. Load case 3.1 was set by anchoring all 6 vertices in the left-top plane and applying a downward 50 N force in the lower right corner (x=20, y=0). Bar stiffness and section were as above. Pre-optimization 10 N tensions lead to central interlacing points in each cube, Figure 9a), vertical displacement of 2.4163 cm at the point of loading, and the largest tension in bar #54 nearing 27 N. Post-structural SA optimization lead to vertical displacement reduced to 2.1071 cm, but increased bar tension to nearing 41 N in bar #54, Figure 9b). Displacement was reduced by 12.80% and length increased by 1.86%, Table 5.

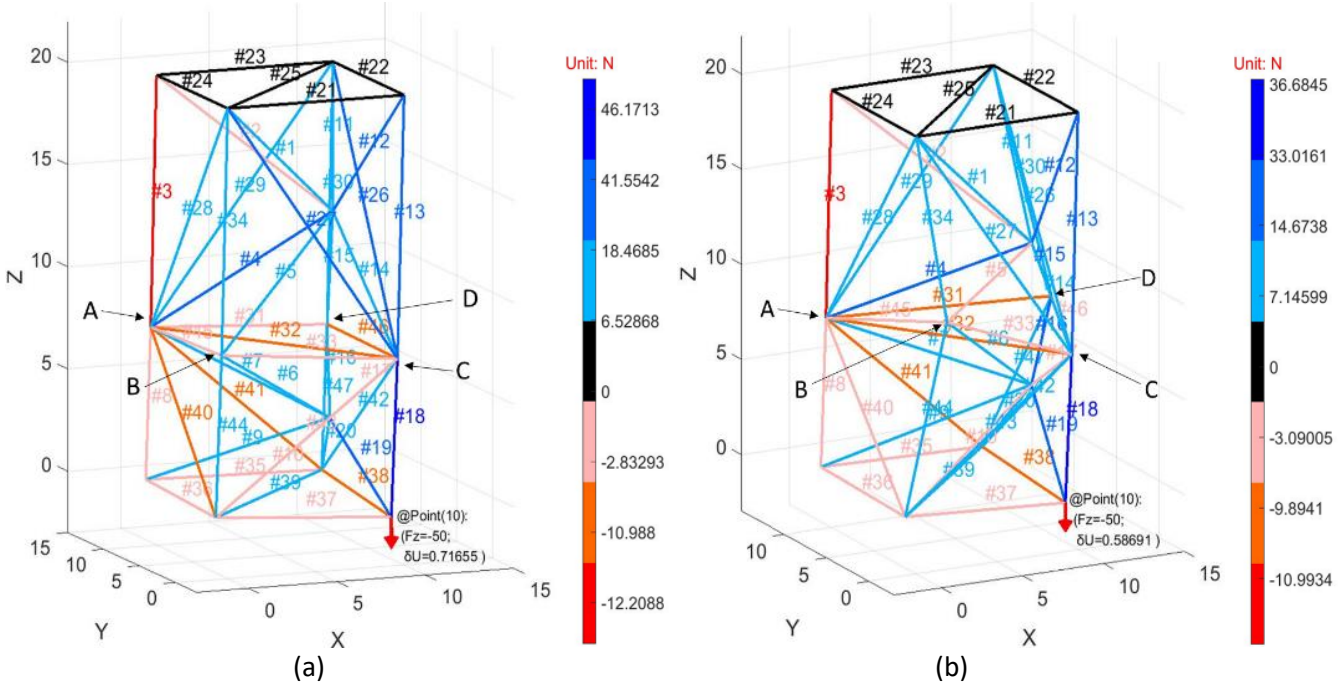

(a) (b)

Figure 7. Displacements and force distributions after optimization for (a) case 3 and (b) trusses

Table 5. Pre-and post-optimization displacements and bar lengths, example 3, load case 1

	Initial, pre-optimization	Optimized-case4	Δ
Applied load 3.1	50 N, vertical down	50 N, vertical down	-
Displacement (cm), load 3.1	2.4163	2.1071	-12.80%
Total bar length (cm), load 3.1	1087.863	1108.125	1.86%

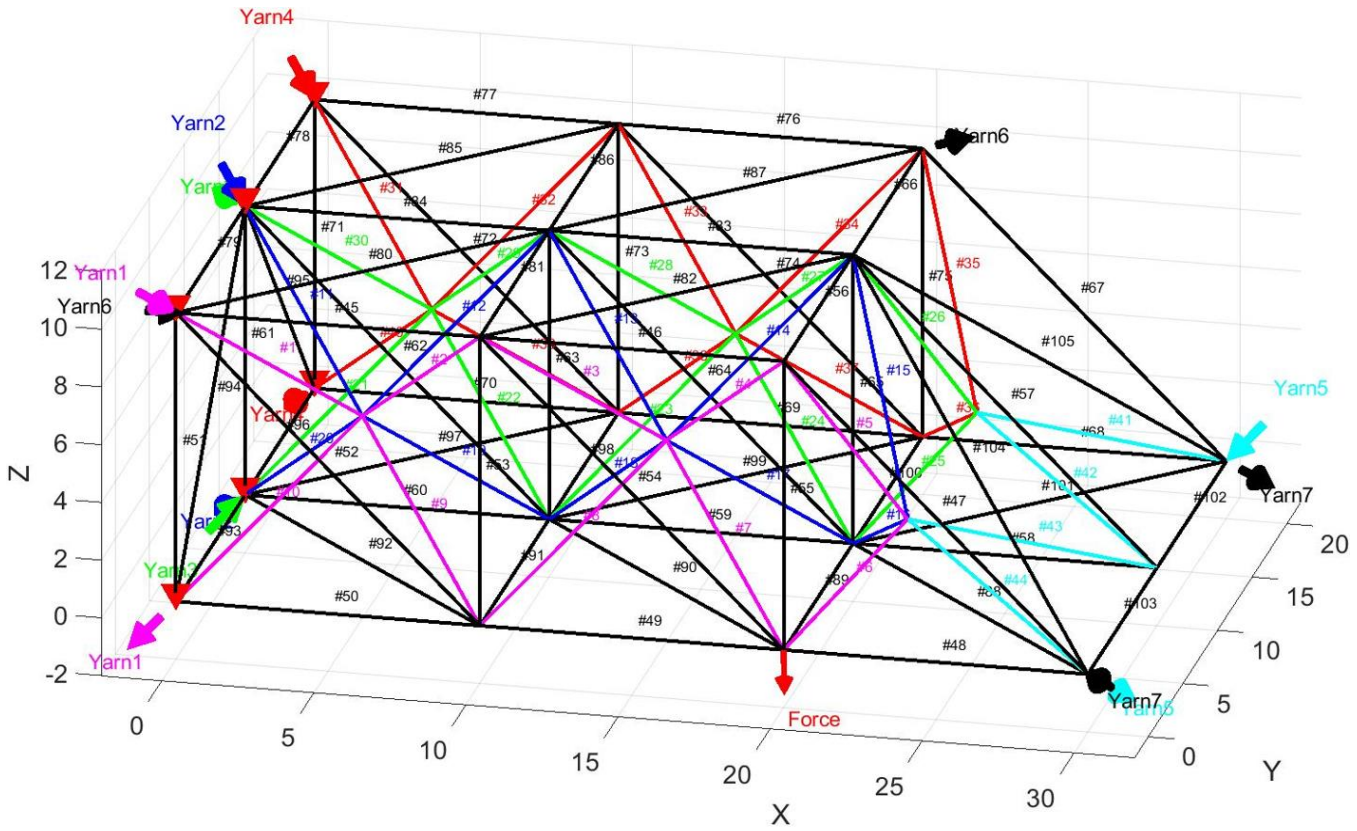

Figure 8. Interlacing diagram for pre-equilibrium 3D structure example 3 featuring 7 yarns and 6 interlacing points

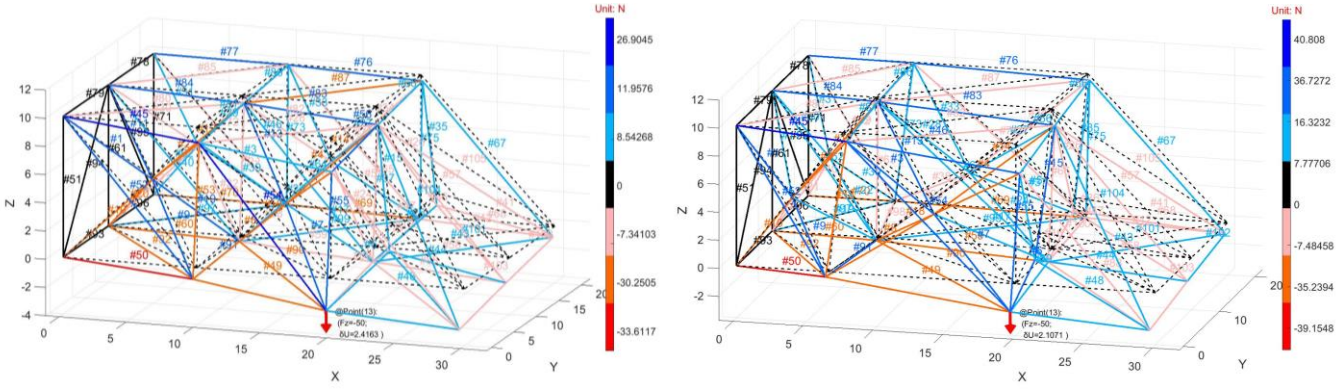

(a) (b)

Figure 9. Displacements and force distributions in non-optimized (a) and optimized (b) part, example 3, load 3.1

5 EXPERIMENTAL

Steepest ascent validation was conducted using a 35 cm side length cubic volume. Two sets of tensions were tested thrice and two interlacing point positions a and b were measured using a MicroScribe G2X contact CMM. Measurements and SA calculations appear in Figure 10. Average consistencies between measured data and SA calculation were 95.4% (tensions case 1) and 95.6% (tensions case 2) at interlacing point a, and 98.3% (tension case 1) and 95.8% (tension case 2) at interlacing point b.

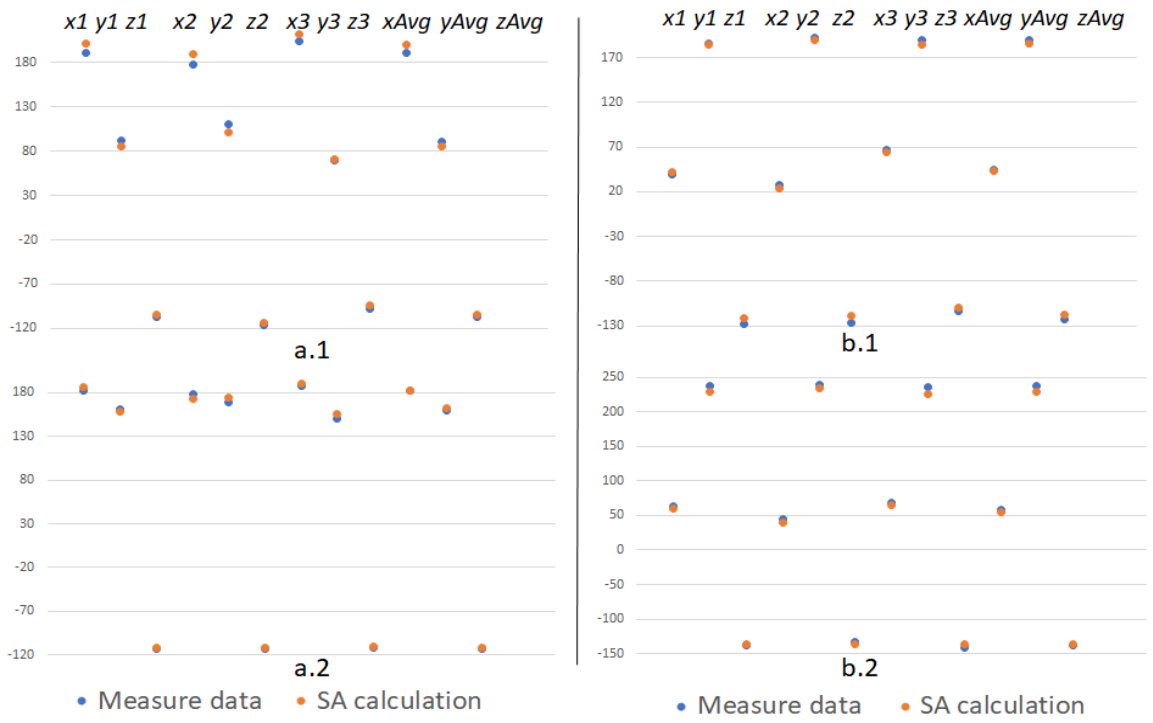

Figure 10. Data consistency for interlacing points a (left) and b (right)

6 CONCLUSION

Future analytical topics of development include optimized/deterministic initial interlacing patterns; management of yarn interference/new interlacing upon tensioning; increased yarn/PMFRC volume ratio; inclusion of PMFRC segment bending and torsion; management of load case spectra. Further experimental topics of development include work on PMFRC open structure manufacturing routes and characterisation of load transfer at interlacing.

7 REFERENCES

[1] J. Plocher and A. Panesar. “Review on design and structural optimisation in additive manufacturing: Towards next-generation lightweight structures”. Materials & Design, V. 183, 108164, 2019.

[2] C.J. Hunt, F. Morabito, C. Grace, Y. Zhao, K. Benjamin and S. Woods. “A review of composite lattice structures”. *Composite Structures,* Vol. 284, 115120, 2022.

[3] A. Forcellese, M. Simoncini, A. Vita and V. Di Pompeo. “3D printing and testing of composite isogrid structures”. *Int J Adv Manuf Technol*, Vol. 109, pp 1881–1893, 2020.

[4] A.V. Azarov, V.A. Kolesnikov and A.R. Khaziev. “Development of equipment for composite 3D printing of structural elements for aerospace applications”. *IOP Conf. Ser.: Mater. Sci. Eng.* 934 012049, 2020.

[5] C.J. Hunt, Y. Zhao, M.R. Wisnom and B.K.S. Woods. “WrapToR composite truss structures: Measurement and modelling of mechanical response”. *Composite Structures*, Vol. 254, 112834, 2020.

[6] L. Sorrentino, M. Marchetti, C. Bellini, A. Delfini and F. Del Sette. “Manufacture of high performance isogrid structure by robotic filament winding”. *Composite Structures*, Vol. 164, pp 43–50, 2017.

[7] R. Schütze. “Lightweight carbon fibre rods and truss structures”. *Materials & Design*, Vol. 18, Nos. 4/6, pp 231-238, 1997.